J. Am. Chem. Soc. **1988**, *110*, 1012–1024

Semiconductor Particles in Bilayer Lipid Membranes. Formation, Characterization, and Photoelectrochemistry

Xiao Kang Zhao, Subhash Baral, Ranieri Rolandi, and Janos H. Fendler*

Contribution from the Department of Chemistry, Syracuse University, Syracuse, New York 13244-1200. *Received May 18, 1987*

Abstract: Bilayer lipid membranes (BLMs) have been formed from bovine brain phosphatidylserine (PS), glyceryl monooleate (GMO), and a polymerizable surfactant, $[n\text{-}C_{15}H_{31}CO_2(CH_2)]_2N^+(CH_3)CH_2C_6H_4CH{=}CH_2,Cl^-$ (STYRS). These BLMs were then used to provide matrices for the in situ generation of microcrystalline CdS, CuS, Cu_2S, PbS, ZnS, HgS, and In_2S_3. Semiconductors were formed by injecting appropriate metal ion precursors and H_2S into the bathing solutions on opposite sides of the BLM. Their presence was established by voltage-dependent capacitance measurements, absorption spectroscopy, and optical microscopy. Subsequent to the injection of H_2S, the first observable change was the appearance of fairly uniform white dots on the black film. These dots rapidly moved around and grew in size, forming islands that then merged with themselves and with a second generation of dots, which ultimately led to a continuous film that continued to grow in thickness. Film formation and growth were monitored by simultaneous optical thickness and capacitance measurements. These data were treated in terms of an equivalent R–C circuit and allowed for the assessment of the semiconductor penetration depth into the BLM. This value for a GMO-BLM-supported In_2S_3 film was determined to be 24 Å. Bandgap excitation, by nanosecond-pulsed or continuous illumination of the BLM-supported semiconductor film, led to observable photoelectric effects. Visible light ($\lambda > 350$ nm) excitation into STYRS-BLM-supported CdS led to the polymerization of the styrene moiety of STYRS. BLM-supported semiconductors remained stable for days. They could be removed from solution and prepared as arrays on a copper grid. Ex situ electron diffraction established a diamond-type cubic lattice with a lattice constant of 5.43 Å for GMO-BLM-supported CdS.

Lipid films of bimolecular thicknesses, bilayer or black lipid membranes (BLMs) as they have become known, have been extensively used in the past two decades as membrane models.[1-3] BLMs are formed at small Teflon orifices (diameters of 2 mm or less) separating two compartments containing aqueous solutions, typically by painting a solution of the lipid in a hydrocarbon solvent across the pinhole. The initially formed film is rather thick. Within minutes it thins and ultimately forms a planar bilayer. During thinning, light reflected from the film changes color as a result of interference, and it eventually turns grayish black. This color corresponds to a single bilayer (40–50 Å thick), hence the name black or bilayer lipid membrane.

Separation of two aqueous solutions by the BLM allows electrical measurements by macroscopic electrodes. Precise capacitance, conductance, and impedance measurements, both in the absence and in the presence of ionophores, have contributed much to our understanding of impulse and ion-transport mechanisms.[4] Particularly significant has been the development of voltage clamping (i.e., holding the bilayer membrane at a predetermined potential and measuring the current flow) and single-channel recording.[5,6]

Investigations of BLMs suffer from two major drawbacks. First, BLMs are notoriously unstable. Very rarely do they survive longer than a couple of hours. Second, voltage clamping provides information only on the transition from an open state to a closed state in ion channels and not to events of the closed states. Current research in our laboratories is directed to overcoming these disadvantages by stabilizing BLMs by polymerization[7] or by polymer coating and by developing simultaneous in situ spectroscopic and electrical techniques[7] for monitoring functioning BLMs. Direct spectroscopic measurements of absorptions provide substantial and much-needed complementary information on the properties of BLMs. Extreme thinness of the BLM renders spectroscopic techniques difficult; absorbances of relatively few molecules need to be determined. Intracavity laser absorption spectroscopy (ICLAS) provided the needed measurements.[8] Absorbances in ICLAS are determined as intracavity optical energy losses. Sensitivity enhancements originate in the multipass, threshold, and mode-competition effects. Thus, for BLM-incorporated chlorophyll *a*, we observed absorbances in the order of 10^{-6}.[8] We have also developed techniques for reflectance measurements and steady-state and subnanosecond time-resolved fluorescence spectroscopy at BLM surfaces.

Concurrent with our developing simultaneous electrical and spectroscopic techniques, studies have been initiated for the incorporation of semiconductor particles into BLMs.[9] Microcrystalline semiconductors have been fruitfully utilized in many photoconversion processes.[10-12] Dispersed microcrystalline semiconductors offer a number of advantages. They have broad absorption spectra, high surface areas, and high extinction coefficients at appropriate band energies. They are relatively inexpensive and can be sensitized by doping (by chemical or physical modifications). Unfortunately, microcrystalline semiconductors also suffer from a number of disadvantages. Until recently they could not be reproducibly prepared as small (less than 20 nm in diameter), monodispersed particles. Small and uniform particles are needed to diminish nonproductive electron-hole recombinations. The smaller the semiconductor particle, the greater the chance of the escape of the charge carriers to the particle surface where electron transfer can occur. There is a minimum size, however, which the particles must reach before absorption occurs at the bulk bandgap (i.e., before the polymolecular cluster becomes a semiconductor). The onset of semiconducting properties for CdS has been estimated to occur for

(1) Tien, H. T. *Bilayer Lipid Membranes (BLM). Theory and Practice*; Dekker: New York, 1974.
(2) Fendler, J. H. *Membrane Mimetic Chemistry*; Wiley-Interscience: New York, 1982.
(3) Miller, C. *Ion Channel Reconstitution*; Plenum: New York, 1986.
(4) Hoppe, W.; Lohmann, W.; Markl, H.; Ziegler, H. *Biophysics*; Springer: New York, 1983.
(5) Sakmann, B.; Neher, E. *Single-Channel Recording*; Plenum: New York, 1983.
(6) Hille, B. *Ionic Channels of Excitable Membranes*; Sinauer: Sunderland, MA, 1984.
(7) Rolandi, R.; Flom, S. R.; Dillon, I.; Fendler, J. H. *Prog. Colloid Polym. Sci.* **1987**, *73*, in press.
(8) Zhao, X. K.; Fendler, J. H. *J. Phys. Chem.* **1986**, *90*, 3886.
(9) (a) Baral, S.; Zhao, X. K.; Rolandi, R.; Flom, S.; Fendler, J. H. Presentation at the Electrochemical Society Meeting, Philadelphia, PA, May 10–15, 1987. Baral, S.; Zhao, X. K.; Rolandi, R.; Fendler, J. H. *J. Phys. Chem.* **1987**, *91*, 2701. (b) Subsequent to the submission of this manuscript, a report describing the deposition of metallic and semiconductor particles on BLMs appeared: Kutnik, J.; Tien, H. T. *Photochem. Photobiol.* **1987**, *46*, 13.
(10) Fox, M. A. *Acc. Chem. Res.* **1983**, *16*, 314.
(11) Grätzel, M. *Energy Sources Through Photochemistry and Catalysis*; Academic: New York, 1983.
(12) Fendler, J. H. *J. Phys. Chem.* **1985**, *89*, 2730.

0002-7863/88/1510-1012$01.50/0

particles whose diameters reach 6 nm.[40] It is difficult to maintain semiconductors in a dispersed state in solution for extended times in the absence of stabilizers. Stabilizers are bound to affect, of course, the photoelectrical behavior of semiconductors. Their modification and their coating by catalysts are, at present, more of an art than a science. Furthermore, the lifetime of electron-hole pairs in semiconductors is orders of magnitude shorter than the excited-state lifetime of typical organic sensitizers. This is due to the much faster electron-hole recombinations in semiconductors than the diffusion-limited quenchings observed with organic sensitizers in homogeneous solutions. Quantum yields for charge separations in colloidal semiconductors are, therefore, disappointingly low.

Some of these difficulties have been overcome by incorporating semiconductor particles into reversed micelles,[13,14] polymer films,[15-19] surfactant vesicles,[20-23] clays,[24,25] vycor glass,[26] and zeolites.[27]

We report here the incorporation of a variety of microcrystalline semiconductor particles into BLMs, the characterization of these systems by electrical, optical, and spectroscopic measurements, and the in situ examination of semiconductor-mediated photoprocesses.

Experimental Section

Materials. $CdCl_2$, $Hg(NO_3)_2$, Cu_2Cl_2, KCl, $ZnCl_2$ (Baker Analyzed Reagents), $InCl_3$ (Alfa Products), $Pb(NO_3)_2$, $CuSO_4$ (Fisher Scientific), $AgNO_3$, $CuCl_2$ (Matheson, Coleman, and Bell), H_2S (Matheson Gas Products), and sodium hexametaphosphate (Sigma Chemical) were used as received. Decane, chloroform, and ethanol solvents (Aldrich Chemical Co.) used to make the lipid-forming solution were of +99% purity and were used as received. Water was purified using a Millipore Milli-Q system provided with a 0.4-μm Millistak filter at the outlet.

Bovine brain phosphatidylserine, PS (Avanti Polar Lipids, Inc.), and glyceryl monooleate, GMO (Nucheck Co.), were used as received. Synthesis, purification, and characterization of polymerizable surfactant, $[n\text{-}C_{15}H_{31}CO_2(CH_2)]_2N^+(CH_3)CH_2C_6H_4CH{=}CH_2,Cl^-$ (STYRS), have been described.[28] PS, GMO, and STYRS were stored at −5 °C in a refrigerator. BLM-forming solutions (50 mg of GMO/1.0 mL of decane, 20 mg of PS/1.0 mL of decane, and 20 mg of STYRS/1.0 mL of decane + 0.010 mL of ethanol) were freshly prepared just prior to their use.

In the case of phosphatidylserine, the chloroform solution (as received) was evaporated by gently passing dry argon over the solution for about 30 min before the required volume of decane was added.

BLM Formation. A thin (0.10–0.15-mm) Teflon film was sandwiched between two 1.00-cm path length, rectangular quartz cells. Contact was made through 6 mm × 15 mm holes drilled through the connecting faces of the two cells and a 1.00-mm-diameter hole punched through the Teflon film clamped between the two cells. The cells were filled with 4.0 mL of 0.10 M aqueous KCl solution at ambient temperature. BLMs were made by "painting" the BLM-forming solution across the 1.00-mm hole separating two compartments. In some cases, particularly for optical experiments when a supporting electrolyte was not needed, pure water was used instead of 0.10 M KCl.

Thinning of the films to 50 ± 5 Å thick black BLMs was monitored by the observation of reflected light (through an Olympus PM-10-M microscope and a 150-W xenon lamp via an optical fiber and a 500-nm cut-off filter) and by capacitance measurements. For optical absorption measurements in conventional spectrophotometry, a vertical array of four BLMs was produced on four 1.0-mm-diameter holes punched in a thin Teflon sheet.

Semiconductor Generation and Monitoring on BLMs. Semiconductors were formed on the BLM by introducing freshly prepared solutions of appropriate metal salt (typically 50 μL of 0.10 M solution, except for Cu_2Cl_2 where a saturated solution in 0.1 M KCl was used) to the cis side of the BLM (containing a 2.0-mL solution of 0.1 M KCl). After 10–15 min of incubation period, 20–25 μL of H_2S gas was slowly injected (over a 2–3-min period) into the trans side of the BLM. Within approximately 5 min, the semiconductor particles became visible on the BLM when observed through the microscope, and the amount and sizes of the particles grew for the next 1–2 h. A slight variation of this procedure gave rise to In_2S_3, CuS, and ZnS semiconductor deposits that looked like continuous film. Thus, injecting a large amount of H_2S to the trans side followed by quick addition of a metal ion on the cis side resulted in the formation of a continuous shining film on the cis side within 20–30 min on the BLM surface. In some cases, the metal–salt solution and H_2S were alternately added in small portions on opposite sides over a period of about 30 min to produce a larger amount of semiconducting material. In all cases, the solutions in the cell remained colorless and optically transparent, and their absorption spectra did not show any presence of semiconductors.

Semiconductor-containing BLMs were found to be more stable than the BLM itself, sometimes remaining intact for days. In a few cases, the aqueous solutions from both sides of the BLM were removed without disturbing the semiconductor deposit on the Teflon support. This allowed ex situ transmission electron microscopy on these semiconductor deposits.

Electron Microscopy. Electron microscopy of microcrystalline semiconductor particles, produced on BLMs, was performed on a RCA EMU-4 electron microscope in the microscope (shadowing) and diffraction mode with a 100-keV electron beam. A 3.0-mm-diameter (200-mesh) copper grid was fixed to a 1.5-mm-diameter hole punched on a 0.1 mm thick Teflon film with a small amount of lipid (GMO). The open holes of the grid (approximately 30–35) were then painted with GMO-BLM-forming solution, and the Teflon film was slowly inserted along the diagonal in a 1-cm path length cuvette containing about 2 mL of water. The dimensions of the Teflon film were such that it fit tightly against the corners and the bottom of the cell, providing two more or less isolated compartments. BLM formation in the squares of the copper grid was monitored by microscopy (Figure 1a). Formation of CdS particles on these GMO BLMs, with procedures already described in the previous section, is shown in Figure 1b. Electron microscopy was performed on much more thinly coated BLMs. Slight tarnishing of the copper grids, due to reaction with H_2S, was also observed (an attempt to use carbon grids to avoid this problem was unsuccessful as BLMs will not form on these weaving grids). Subsequent to deposition, the Teflon film was slowly lifted out of the cell. For ZnS and In_2S_3, the semiconductor film was initially formed on the hole of a Teflon film and then transferred to the copper grid by floating it on water. The diffraction patterns were indexed by a camera constant determined from the pattern of a standard gold film recorded under identical conditions.

Refractive Index Measurements. Refractive index measurements were made on continuous semiconductor films of In_2S_3 and ZnS generated in situ on GMO BLMs. The BLM-supported semiconductor films were formed across a 1.0-mm-diameter hole on a Teflon film sandwiched between two triangular quartz cells. Contact was made through 7 mm × 20 mm holes drilled through the connecting hypotenuse faces of the two quartz cells. The entire cuvette assembly (Figure 2a) was mounted on a small, precision rotating optical stage. The BLM-supported semiconductor film was illuminated by a He–Ne laser light (6328 Å), which was polarized parallel to the plane of incidence. The beam was focused on a small portion at the middle of the BLM containing the semiconductor film. The reflected light intensity was measured with a Spectra Physics Model 404 silicon photocell power meter fitted with a polarizer to eliminate any perpendicularly polarized light. The value of the Brewster angle was obtained from the angle of incidence and the angle of emergence read directly from the graduated scale of the precision optical stages when the intensity of the reflected light is zero (minimum). The refractive index was calculated from the Brewster angle by relationships discussed later.

Simultaneous Reflectivity, Capacitance Measurements, and Color Observations. The previous setup described for refractive index measurements was modified (Figure 2b) to allow simultaneous capacitance and

(13) Meyer, M.; Wallberg, C.; Kurihara, K.; Fendler, J. H. *J. Chem. Soc., Chem. Commun.* **1984**, 90.
(14) Lianos, P.; Thomas, J. K. *Chem. Phys. Lett.* **1986**, *125*, 299.
(15) Meissner, D.; Memming, R.; Kastening, B. *Chem. Phys. Lett.* **1983**, *96*, 34.
(16) Krishnan, M.; White, J. R.; Fox, M. A.; Bard, A. J. *J. Am. Chem. Soc.* **1983**, *105*, 7002.
(17) Mau, A. W. H.; Huang, C. B.; Kakuta, N.; Bard, A. J.; Campion, A.; Fox, M. A.; White, M. J.; Webber, S. E. *J. Am. Chem. Soc.* **1984**, *106*, 6537.
(18) Tien, H. T.; Bi, Z. C.; Tripathi, A. K. *Photochem. Photobiol.* **1986**, *44*, 779.
(19) Kuczynski, J. P.; Milosavljevic, B. M.; Thomas, J. K. *J. Phys. Chem.* **1984**, *88*, 980.
(20) Tricot, Y.-M.; Fendler, J. H. *J. Am. Chem. Soc.* **1984**, *106*, 2475. Tricot, Y.-M.; Fendler, J. H. *J. Am. Chem. Soc.* **1984**, *106*, 7359.
(21) Tricot, Y.-M.; Emeren, A.; Fendler, J. H. *J. Am. Chem. Soc.* **1985**, *89*, 4721.
(22) Rafaeloff, R.; Tricot, Y.-M.; Nome, F.; Tundo, P.; Fendler, J. H. *J. Phys. Chem.* **1985**, *89*, 1236.
(23) Youn, H. C.; Tricot, Y.-M.; Fendler, J. H. *J. Phys. Chem.* **1987**, *91*, 581.
(24) Enea, O.; Bard, A. J. *J. Phys. Chem.* **1986**, *90*, 301.
(25) Stramel, R. D.; Nakamura, T.; Thomas, J. K. *Chem. Phys. Lett.* **1986**, *130*, 43.
(26) Kuczynski, J.; Thomas, J. K. *J. Phys. Chem.* **1985**, 2720.
(27) Wang, Y.; Herron, N. *J. Phys. Chem.* **1987**, *91*, 257.
(28) Reed, W.; Guterman, L.; Tundo, P.; Fendler, J. H. *J. Am. Chem. Soc.* **1984**, *106*, 1897.

reflectance measurements and color observations on a BLM-supported semiconductor film during its formation and thickening. The incident beam from the He–Ne laser was polarized perpendicularly to the incident plane for this experiment and made an incident angle of 30° with the quartz cell surface. The intensity of the beam reflected from the semiconductor film was continuously monitored and recorded at the same angle. Determination of the color of the film was made by visual observation and photography of the 90° reflected light (by the film) from a 150-W xenon lamp guided through an optical fiber and a shutter. A pair of Ag/AgCl electrodes immersed in the bathing solutions across the BLM were connected to a computer-interfaced precision RLC Digibridge (GR 1689, Genrad Corp.), which continuously recorded the capacitance of the semiconductor-containing BLM.

Conductance, Capacitance, and Voltage-Dependent Capacitance Measurements. Electrical measurements were taken via two Ag/AgCl (0.10 M KCl) electrodes immersed into the cis and trans sides of the BLM in an electrically isolated cell.

For voltage-dependent capacitance measurements, the Ag/AgCl electrodes were connected via a 0.1-GΩ headstage (Model 8910, Dagan Corp.) set at a gain of 0.5 mV/pA with a filter of 1 kHz. A Hewlett-Packard 8116A pulse function generator provided a bipolar triangular wave, dV/dt = 16 mV/12.5 ms, for the stationary capacitance measurements and a dc offset, V, as an externally applied electric potential. The output of the patch clamp was recorded on a Tektronix 2215A oscilloscope set at the x–y mode. Experimental points reported at different applied voltages were the mean of at least four measurements performed sequentially at increasing and decreasing voltages (to compensate for possible hysteresis). Solvent-containing BLMs required a long time (2–20 min) to reach steady-state values of capacitance.[29]

Photoelectric Effect Measurements. Figure 3 shows the schematics of the experimental setup used for photovoltage and photocurrent measurements. Two pairs of Ag/AgCl electrodes, carefully shielded by black Teflon tubes (to minimize the generation of light-induced electrode potentials), were immersed into the cells. A pair of electrodes were connected, via the 8910 probe (0.1-GΩ feedback) or the 8920 probe (1.0-GΩ feedback), to the 8900 patch clamp, either setting the filter at wide-band position and high-frequency boost (for photocurrent measurements) or holding potential at an appropriate dc voltage (maximum ±20 mV) to compensate for spurious potentials generated by offset currents across the membrane (during photovoltage measurements). The second pair of electrodes were connected to a Keithley Model 602 electrometer with an input impedance of 10^{14} Ω as a voltmeter or with an input impedance of 10^{7} Ω as an ammeter operating at fast mode. Outputs from the patch clamp or from the electrometer were connected to a Tektronix 4662 storage oscilloscope via a three-position switch. When a photovoltage signal greater than 1 mV was measured, the input of the oscilloscope was connected directly with the pair of electrodes originally connected to the electrometer in order to improve the response time. Electrical signals greater than 1 mV were photographed on the oscilloscope. Signals lower than 1 mV were preamplified and transferred to a Zenith Data System computer (Z-100) via a programmable digitizer (390 AD, Sony-Tektronix) to be stored and averaged. The response times were 10^{-8} s (photovoltage) and 10^{-6} s (photocurrent), and the sensitivities (signal: noise = 2:1, single shot) were 10^{-5} V (photovoltage) and 10^{-13} A (photocurrent).

Photoeffects were initiated by 20-ns laser pulses, obtained by focusing the third (353.4-nm) harmonic of a Quanta Ray DCR-1 Nd-YAG laser onto the middle of the BLM by plano-convex, fused-silica lenses (focal length 50 cm). The oscilloscope single scanning was synchronized with the laser pulse via a Trigger and Digital Delay Generator (Model III AR) with nanosecond accuracy. The energy of the laser pulse was varied by neutral density filters and determined by means of a Scientech 3652 power/energy meter. Blank measurements in the absence of semiconductors on the BLM and with broken BLMs were routinely performed.

Photopolymerization. The photopolymerization experiments were done on a vertical array of four BLMs produced on four 1.0-mm-diameter holes punched on a 0.1 mm thick Teflon strip. The holes were painted with a small amount of lipid-forming solution from STYRS surfactant. The strip was then vertically inserted into a cuvette containing about 2 mL of 1×10^{-4} M solution of CdS colloid stabilized with 1×10^{-4} M sodium hexametaphosphate at pH 6 (prepared by a method described previously[30]) and positioned on the sample beam path of the spectrophotometer. After the lipid films were thinned out to form BLMs, they were irradiated with light coming from a 150-W xenon lamp filtered with a 350-nm cut-off filter through an optical fiber guide. The progress of polymerization was monitored by scanning the absorption spectra of the BLMs at every 2-min intervals during irradiation (a CdS solution of the same concentration was used as reference). Precautions were taken to avoid excess irradiation of the BLMs by the probing beam of the spectrophotometer. Irradiations at wavelengths greater than 350 nm in control experiments in the absence of CdS particles did not lead to polymerization. Conversely, BLM polymerization was observed, in the absence of CdS, upon irradiation by ultraviolet light.[7]

Results and Discussion

Microcrystalline cadmium, mercury(II), copper(I), copper(II), indium, zinc, lead, and silver sulfides were generated in situ or deposited on bilayer lipid membranes (BLMs) prepared from bovine brain phosphatidylserine (PS), glyceryl monooleate (GMO), and a synthetic, polymerizable surfactant, [n-$C_{15}H_{31}CO_2(CH_2)]_2N^+(CH_3)CH_2C_6H_4CH{=}CH_2,Cl^-$ (STYRS). Semiconductor formation and growth on the BLMs have been monitored by electrical, optical, and spectroscopic measurements, by visual observations and photomicrography.

Voltage-dependent capacitance measurements have been utilized for monitoring surface potential changes of BLMs prepared from PS prior and subsequent to cadmium ion adsorption and CdS formation. The ease of formation, stability, and available information[1,3] prompted the selection of GMO BLMs for most of our experiments. Similarly, previous experience in our laboratory led to STYRS photopolymerization[28,31] for demonstrating a semiconductor-mediated reaction in the matrix of a BLM.

Voltage-Dependent Capacitance Measurements. Determination of surface-potential changes on charged-BLM surfaces provides an adsorption-sensitive method for monitoring semiconductor formation and adsorption of its metal ion precursor. The surface charge density, σ, is related to the surface potential, ψ, by the Gouy–Chapman theory (eq 1), where k is the Boltzmann constant,

$$A\sigma/C^{1/2} = \sinh(ze\psi/2kT) \quad (1)$$

T is the absolute temperature, e is the electronic charge, z is the valence of the symmetrical electrolyte in the solution, and C is the bulk aqueous electrolyte concentration. $A = 1/(8N\epsilon_m\epsilon_0 kT)^{1/2}$ where N is Avogadro's number. ϵ_m is the dielectric constant of the BLM, and ϵ_0 is the permittivity of free space.[32] From eq 1, the charge density can be computed if the surface potential is known. BLM surface potentials can be conveniently determined by voltage-dependent capacitance measurements.[33,34] Advantage is taken, in this method, of electric field induced geometrical changes of the BLM, sometimes referred to as electrocompression or electrostriction,[35-39] which manifest in voltage-dependent membrane capacitances.

The electric field acting on the bilayer is composed of two components: the externally applied field, V, and the intrinsic field, due to the potential difference between the two surfaces of the BLM, $\Delta\psi$. The capacity–voltage relationship is given by eq 2,[33,34]

$$\frac{C(V) - C(0)}{C(0)} = \alpha(\Delta\psi + V)^2 + U \quad (2)$$

where $C(V)$ and $C(0)$ are the capacitances at applied voltage of V and zero, respectively, α is a proportional factor, and U is a constant related to reference capacity. Equation 2 shows that, for an asymmetrical BLM, there exists an applied voltage, V_{min} (called capacitance minimization potential), when the first term

(29) Weaver, J. C.; Powell, K. T.; Mintzer, R. A.; Ling, H.; Sloan, S. R. *Bioelectrochem. Bioenerg.* **1984**, *12*, 393.
(30) Fojtik, A.; Weller, H.; Koch, U.; Henglein, A. *Ber. Bunsen-Gew. Phys. Chem.* **1984**, *88*, 969.
(31) Fäldt, P.; Youn, H. C.; Baral, S.; Zhao, X. K.; Fendler, J. H., unpublished results, 1986.
(32) McLaughlin, S. In *Current Topics in Membranes and Transport*; Bonner, F., Kelinzeller, A., Eds.; Academic: New York, 1977; Vol. 9, p 71.
(33) Alvarez, O.; Latorre, R. *Biophys. J.* **1978**, *21*, 1.
(34) Usai, C.; Marcetti, C.; Gambale, F.; Robello, M.; Gorio, A. *FEBS Lett.* **1983**, *153*, 315.
(35) Babakov, A. V.; Ermishkin, L. N.; Liberman, E. A. *Nature (London)* **1966**, *210*, 953.
(36) White, S. H. *Biophys. J.* **1970**, *10*, 1127.
(37) Schoch, P.; Sargent, D. F. *Experientia* **1976**, *32*, 811.
(38) Benz, R.; Beckers, F.; Zimmermann, U. *J. Membr. Biol.* **1979**, *48*, 181.
(39) Schoch, P.; Sargent, D. F.; Schwyzer, R. *J. Membr. Biol.* **1979**, *46*, 71.

of the left side becomes zero; i.e., $V_{min} = -\Delta\psi$. If ψ_c and ψ_t are the electrostatic potentials due to the charge densities, σ_c and σ_t at the cis and trans surfaces of the BLM, respectively, we have $V_{min} = \psi_c$, as under our experimental conditions,[34] $\psi_t = 0$ ($\sigma_t = 0$). Therefore, the measured value of V_{min} allows the calculation of σ_c from eq 1.

Figure 4 shows the measured capacity–voltage curves for a BLM prepared from PS in the absence of any additives (curve a), subsequent to the addition of $CdCl_2$ to the cis side of the BLM to generate 5.0×10^{-4} M $CdCl_2$ (curve b), and subsequent to the injection of H_2S to the trans side to give 3.4×10^{-4} M H_2S (curve c). Curve a is symmetrical about the axis of zero applied voltage, as expected for membranes with $\Delta\psi = 0$. Positively charged cadmium ions were electrostatically attracted to the cis surface of the negatively charged PS BLM. This resulted in partial charge neutralization at one side of the membrane only, hence in the generation of a transmembrane potential. In accordance with this, V_{min} in curve b is seen to have shifted along the voltage axis by an amount needed to compensate for the BLM asymmetry. This amount, $V_{min} = 66$ mV, is comparable to that reported on the addition of 5.0×10^{-4} M $CaCl_2$ to the cis side of a symmetrical PS BLM (80 ± 5 mV).[34] Substituting the obtained $V_{min} = 66$ mV and the value of $A = 136.4$ at 22 °C[32] into eq 1 led to $\sigma_c = {}^1/_{360}$ Å^{-2}. A knowledge of the BLM area (S, determined to be 4.4×10^{13} Å^2) allowed the assessment of the number of surface charges, q, on the BLM from eq 3.

$$q = \sigma_c S = 4.4 \times 10^{13}\ \text{Å}^2 \frac{1}{360\ \text{Å}^2} = 1.2 \times 10^{11} \qquad (3)$$

Subsequent to H_2S addition to the trans side of the BLM, $\Delta\psi$ decreased from 66 to 0 mV (curve c in Figure 4), indicating the formation of CdS in the BLM. Assuming a quantitative formation, the number of CdS molecules present in the PS BLM is 6×10^{10} ($q/z = 1.2 \times 10^{11}/2 = 6 \times 10^{10}$). Assuming further that the head group areas of PS are 60 Å^2,[29] the total number of PS molecules on one side of the BLM is $(4.4 \times 10^{13})/60 = 7.3 \times 10^{11}$, and the ratio of CdS to PS is, therefore, 1:12 at the earliest stages of semiconductor formation.

Voltage-dependent capacitance measurements were rationalized in terms of particle formation on the BLMs. Additional experiments, described subsequently, provided an insight into the mechanism of particle formation and growth and established the semiconducting behavior.

Absorption Spectroscopy. Semiconductor formation on BLM surfaces manifested in such a lowering of the amplification in the ICLAS experiments[8] that lasing stopped.

Absorption spectra of microcrystalline semiconductors could be observed, however, on the vertical array of four BLMs. Time evolution of the absorption spectra was recorded for CdS, In_2S_3, ZnS, CuS, Cu_2S, PbS, HgS, and AgS. Information was deduced, in some cases, on the sizes of the initial nuclei formed, as well as on their subsequent agglomeration. Figure 5 shows that, with small amounts of $CdCl_2$ and H_2S, the particles formed at the very beginning (curves 1–4) have absorption edges between 350 and 370 nm and band maxima at ~320 nm. Such a spectrum corresponds to CdS particles[40] of about 18–20-Å diameter. However, these particles kept growing, and after about 10 min, the spectra of the deposit became indicative of bulk macroscopic CdS semiconductors with bandgaps of 2.4 eV and absorption edges of 520 nm. Using a larger amount of $CdCl_2$ and H_2S resulted in faster and larger accumulation of macroscopic semiconductors, as shown in the inset of Figure 5.

Time evolution of absorption spectra (Figure 6) also gave the rate of semiconductor formation on the BLM, which was essentially limited by the permeation of H_2S through the BLM from the trans to the cis compartment. From Figure 6, the CdS formation under the experimental condition was found to initially follow simple, monoexponential kinetics and was essentially complete in about 3 h. A permeation rate of 1×10^{-7} M s^{-1} can be calculated for H_2S through the GMO BLM at the beginning when the H_2S concentration on the trans side was 3×10^{-4} M.

Similar absorption spectra were taken for In_2S_3 (Figure 7) and PbS (Figure 8). These semiconductors correspond in the bulk state to bandgaps of 2.0 (620) and 0.4 eV (>1000 nm).[41] Addition of H_2S to an aqueous solution of $InCl_3$ or $Pb(NO_3)_2$ resulted in the immediate formation of particles with absorption edges of 610 and >800 nm, respectively. However, the spectra of the semiconductors formed in situ in GMO BLMs showed the presence of lower wavelength absorption bands (at 270 and 400 nm for In_2S_3 and PbS, respectively) in both cases, in addition to broader absorption edges corresponding to the macroscopic semiconductor particles. It is tempting to attribute the low-wavelength absorptions in these cases to the formation of very small sized (Q-particles) particles[42,43] or to the presence of two-dimensional growth.

Other semiconductors, like ZnS and HgS, gave rise to spectra where the absorption edges corresponded closely to the macroscopic bandgaps from the very beginning of the deposition.

Electron Microscopy. CdS deposits were found to be microcrystalline with aggregated clusters (Figure 9a) mostly ranging in size from 800 to 1000 Å. In the background of these big clusters, some very small particles of diameter ~100 Å were also observed. These smaller particles appeared to be initially formed individual crystallites, which then agglomerated to bigger microcrystalline clusters. Enlargement of the shadow of these agglomerates clearly showed the fractal nature of their growth, indicating that the microcrystalline clusters grew by a two-dimensional, diffusion-limited aggregation process from a large number of nuclei on the BLM. The microcrystalline nature of the aggregates was obvious from their electron diffraction pattern (Figure 9b). The Bragg angles were calculated from the diffraction pattern (in Figure 9b) with a camera constant derived from the diffraction pattern of a standard gold film obtained under identical settings of the microscope. The diffraction rings were indexed as (111), (220), (311), (400), (422), (440), and (710, 550, 543), respectively, for a diamond-type cubic lattice with a lattice constant of 5.43 Å. This value is in good agreement with that reported (5.41 Å) for cubic CdS structures.[44] The In_2S_3 films (thickness 1000–1500 Å) were found to be too opaque toward 100-keV electron beam. Their shadows, however, were found to be of a continuous nature without any discernible hole (Figure 9c). Their crystalline nature is indicated by the sharp edges observed where the films were fractured either by mechanical means or by focusing the electron beam very strongly on a small area.

Optical Microscopy. A wealth of information was obtained by monitoring the growth of microcrystalline semiconductor particles on BLMs by optical microscopy and photomicrography. Subsequent to the injection of H_2S, the first observable change was the appearance of fairy uniform white dots of 1 μm or less on the black film (see photograph a in Figure 10). These corresponded to curve 2 in Figure 5 in the absorption spectra and, most presumably, were the smaller particles of ~100-Å diameter observed in the TEM (Figure 9a). The initially formed white dots moved around on the BLM surface, encountering the Plateau–Gibbs border and each other with resulting coalescence, particle growth, and island formation (see photograph b in Figure 10). The islands themselves merged and, concurrently, a second generation of white dots began to appear on the surfaces of the black channels that surrounded the enlarged white islands. The behavior of the second generation dots was similar to that of their predecessors. They rapidly moved around, combined with each other, and ultimately coalesced into

(40) Weller, H.; Schmidt, H. M.; Koch, U.; Fojtik, A.; Baral, S.; Henglein, A.; Kunath, W.; Weiss, K.; Dieman, E. *Chem. Phys. Lett.* **1986**, *124*, 557. Brus, L. E. *J. Chem. Phys.* **1983**, *79*, 5566.

(41) Phillips, J. C. *Bonds and Bands in Semiconductors*; Academic: New York and London, 1973.

(42) Nozik, A. J.; Williams, F.; Nenadovic, M. T.; Rajh, T.; Micic, O. I. *J. Phys. Chem.* **1985**, *89*, 397.

(43) Beebe, T. P., Jr.; Yates, J. T., Jr. *J. Phys. Chem.* **1987**, *91*, 254.

(44) Abrikosov, N. Kh.; Bankina, V. F.; Poretskaya, L. V.; Shelimova, L. E.; Skudnova, E. V. In *Semiconducting II-VI, IV-VI, and V-VI Compounds*; Plenum: New York, 1969.

the surrounding islands (see photograph c in Figure 10). For In_2S_3, ZnS, CuS, and Cu_2S, a continuous film eventually formed, the appearance of which was either that of a shiny, cloudlike layer (10d) or that of a light, foglike grain layer (10e). In some instances, the continuous film formed, pressed against the Plateau–Gibbs border, and overlapped each other. This process could lead to films of several overlapping layers, which manifested in color development (10f). Color formation, albeit with less hue, could also accompany the coalescence of islands (10g and 10h). In general, a single layer of quickly formed film was less thick than the arrested islands of particles. It needs to be emphasized that semiconductor particles, at all stages of their growth, were supported by bimolecular (black) membranes.

It is interesting to note that thin-film growth, observed electron microscopically and modeled by different theories, was discussed in terms of sequential nucleation, giving rise to islandlike structures, coalescence of the islands, channel formation, and development of the continuous film.[45]

Refractive Index Measurements. Brewster angles of GMO-BLM-supported, continuous semiconductor films were measured by the triangular cell setup described in the Experimental Section. The angles of incidence of the laser beam, i and i', in the reversible directions $\vec{A}$ and $\vec{B}$ at which the intensity of the reflected light is zero, are delineated in Figure 2a. The Brewster angle, Θ_B, is given by eq 4. For small i and i' values, eq 4 simplifies to eq 5.

$$\Theta_B = 45° + \frac{1}{2}\left[\sin^{-1}\left(\frac{\sin i}{n_a}\right) + \sin^{-1}\left(\frac{\sin i'}{n_a}\right)\right] \quad (4)$$

$$\Theta_B = 45° + \frac{1}{2n_a}(i + i') \quad (5)$$

Then, the refractive index of a homogeneous isotropic thin film, n_s, immersed in a medium of refractive index n_a (see Figure 2c for definitions) is given by eq 6. Determined values of n_s for

$$n_s = n_a \tan \Theta_B \quad (6)$$

GMO-supported In_2S_3 film as a function of its growing time are shown in Figure 11. Initially, n_s increased exponentially, indicating that the BLM surface coverage was not complete by the In_2S_3 and that the refractive index of the BLM partially contributed toward the measured value at those times. At point D, the BLM surface became fully covered (the film became continuous), and the refractive index, n_s, became time invariant. These values were found to be 1.86 and 1.58 for In_2S_3 and ZnS, respectively.

Simultaneous Optical Thickness and Capacitance Measurements during the Growth of a BLM-Supported, Continuous Semiconductor Film. Figure 2c shows the schematics of two-beam optical interference on a semiconductor-containing BLM. The system is considered to have a three-layer structure, with refractive indices due to the aqueous solution, n_a, the semiconductor layer, n_s, and the BLM, n_m. The optical path length difference between the two reflection beams (R_{as} and R_{sm} in Figure 2c) originating at the aqueous solution–semiconductor and semiconductor–BLM interfaces is given by eq 7, where N_i is an integral number resulting

$$N_i\lambda = 2n_s d_s \cos \Theta_s \quad (7)$$

in constructive interference (i.e. fringe maxima) or half-integer resulting in destructive interference (i.e. fringe minima), λ is the wavelength of the light, d_s is the semiconductor layer thickness, and Θ_s is the angle of refraction in the semiconductor film, related to Θ_a (angle of incident light) by Snell's Law (eq 8). The thickness

$$n_a \sin \Theta_a = n_s \sin \Theta_s \quad (8)$$

of the BLM-supported semiconductor layer is given more accurately by eq 9,[46-48] where Δt_ϕ and Δt_r are phase-shift and reflectivity corrections, which can be estimated by using equations describing the reflectivity of a semiconductor film on a reflective BLM. The boundary conditions for the solution of Maxwell's equations permit the use of Fresnel's formula to compute the reflectance.

$$d_s = N_i\lambda/(2n_s \cos \Theta_s) + \Delta t_\phi + \Delta t_r \quad (9)$$

The reflectance of light polarized perpendicularly to the plane of incidence is given by[49,50]

$$R_\perp = \frac{\gamma_{as}^2 + \gamma_{sm}^2 + 2\gamma_{as}\gamma_{sm} \cos (2\beta - \phi_{sm})}{1 + \gamma_{as}^2\gamma_{sm}^2 + 2\gamma_{as}\gamma_{sm} \cos (2\beta - \phi_{sm})} \quad (10)$$

where

$$\gamma_{as}^2 = \left(\frac{n_a \cos \Theta_a - n_s \cos \Theta_s}{n_a \cos \Theta_a + n_s \cos \Theta_s}\right)^2 \quad (11)$$

and

$$\gamma_{sm}^2 = \frac{(n_s \cos \Theta_s - u_m)^2 + v_m^2}{(n_s \cos \Theta_s + u_m)^2 + v_m^2} \quad (12)$$

are the reflectivities at aqueous solution–semiconductor film interface and at semiconductor film–BLM interface, respectively.

$$\phi_{sm} = \tan^{-1}\left[\frac{-2v_m n_s \cos \Theta_s}{u_m^2 + v_m^2 - n_s^2 \cos^2 \Theta_s}\right] \quad (13)$$

Equation 13 is the phase change at the semiconductor film–BLM interface, where eq 14–17 define variables and k_m is the extinction coefficient of the BLM at the wavelength λ.

$$2u_m^2 = w + (w^2 + 4n_m^2k_m^2)^{1/2} \quad (14)$$

$$2v_m^2 = -w + (w^2 + 4n_m^2k_m^2)^{1/2} \quad (15)$$

$$w = n_m^2 - k_m^2 - n_a^2 \sin^2 \Theta_a \quad (16)$$

$$\beta = 2\pi d_s n_s (\cos \Theta_s/\lambda) = N_i\pi \quad (17)$$

The reflectance minima as given by eq 10 does not coincide with those determined by eq 7; the factors γ_{as} and γ_{sm} vary with the angle of incidence, Θ_a, and give rise to reflectivity corrections. The presence of ϕ_{sm} in the cos $(2\beta - \phi_{sm})$ term leads to the phase-shift thickness correction as shown in eq 18. When the

$$\Delta t_\phi = -(1/2 - \phi_{sm}/2\pi)\frac{\lambda}{2n_s \cos \Theta_s} \quad (18)$$

BLM does not absorb light at wavelength λ, the extinction coefficient, k_m, is zero. Then,

$$v_m = 0 \qquad \phi_{sm} = 0$$

and eq 10, 12, and 18 can be simplified to give eq 19–21.

$$R_\perp = \frac{\gamma_{as}^2 + \gamma_{sm}^2 + 2\gamma_{as}\gamma_{sm} \cos 2\beta}{1 + \gamma_{as}^2\gamma_{sm}^2 + 2\gamma_{as}\gamma_{sm} \cos 2\beta} \quad (19)$$

$$\gamma_{sm}^2 = \left[\frac{n_s \cos \Theta_s - (n_m^2 - n_a^2 \sin^2 \Theta_a)^{1/2}}{n_s \cos \Theta_s + (n_m^2 - n_a^2 \sin^2 \Theta_a)^{1/2}}\right]^2 \quad (20)$$

$$\Delta t_\phi = -\frac{\lambda/2}{2n_s \cos \Theta_s} \quad (21)$$

The phase-shift thickness correction (eq 18) shows that the light

(45) Maissel, L. I., Glang, R., Eds. *Handbook of Thin Film Technology*; McGraw-Hill: New York, 1970; Chapter 8.

(46) Blodgett, K.; Langmuir, I. *Phys. Rev.* **1937**, *51*, 964.

(47) Wesson, R. A.; Phillips, R. P.; Pliskin, W. A. *J. Appl. Phys.* **1967**, *38*, 2455.

(48) Wesson, R. A.; Young, H. W.; Pliskin, W. A. *Appl. Phys. Lett.* **1967**, *11*, 105.

(49) Born, M.; Wolf, E. *Principles of Optics*, 3rd revised ed.; Pergamon: Oxford, 1965; p 632.

(50) American Institute of Physics Handbook, 2nd ed.; McGraw-Hill: New York, 1963; p 6.

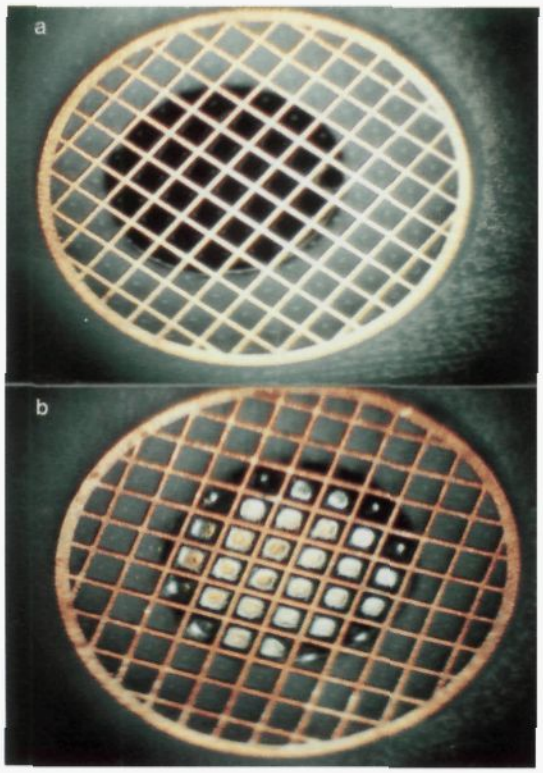

Figure 1. (a) GMO-BLMs on a 200-mesh, 3-mm-diameter, general-purpose copper grid, formed by painting the grid, supported on a thin Teflon film, with BLM-forming solution. (b) CdS deposited on these BLMs by injecting $CdCl_2$ and H_2S in the bathing solutions on opposite sides. The slight tarnishing of the shining copper color of the grid was caused by the H_2S. After deposition, such grids were taken out of the solution and used for ex situ electron microscopy.

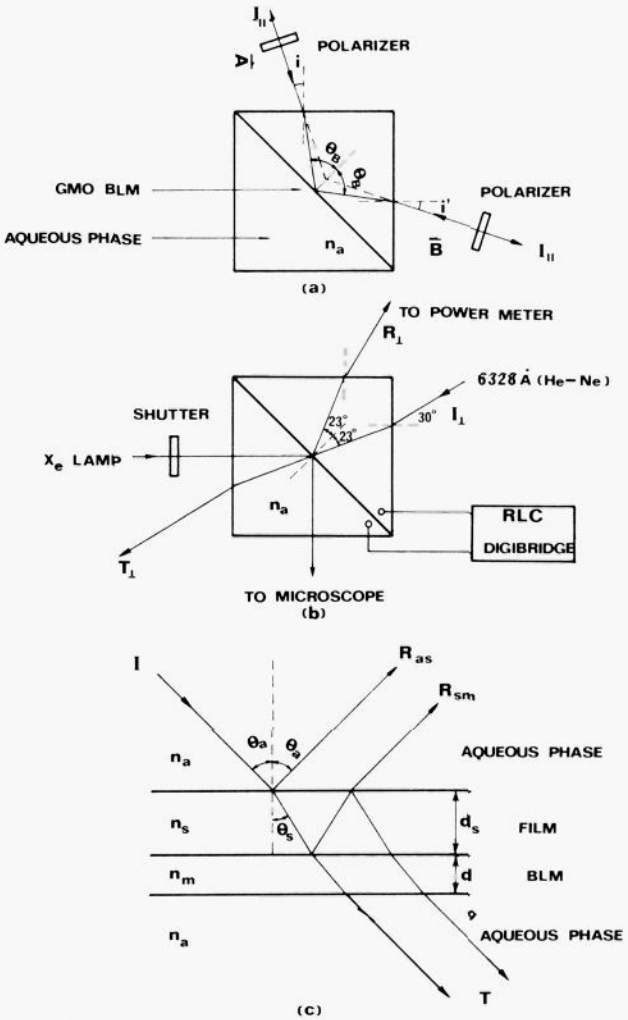

Figure 2. (a) Schematic diagram for Brewster angle (Θ_B) and refractive measurement setups. A cross section of the cells by the plane of incidence is also shown. The laser beam was focused on the middle of the BLM. The cells were mounted on a rotating optical stage. n_a is the refractive index of the aqueous phase. (b) Schematic diagram for simultaneous optical thickness, electrical capacitance, and color observation setup (see the Experimental Section for details). (c) Schematic diagram for two-beam reflection interference occurring on the two interfaces of a semiconductor-containing BLM. The refractive indices of aqueous KCl solution (n_a) and BLM (n_m) were taken as 1.34 and 1.41, respectively. n_s represents the refractive index of the semiconductor experimentally determined by the setup shown in a. d_s and d represent the thicknesses of the semiconductor film and BLM, respectively.

reflected from the aqueous solution–semiconductor film interface suffers a 180° phase shift since the refractive index of the film, n_s, is greater than that of aqueous solution, n_a, whereas the light reflected from the semiconductor film–BLM interface does not undergo change in phase for $n_s > n_m$. The total phase-shift thickness correction was the path length difference corresponding to a 180° phase lag (eq 21), i.e. to half-integral values. The fringe maxima and minima in eq 7 are shifted by half-integers; i.e., when N_i becomes a half-integer, brightness results from constructive interference, while when N_i becomes an integer, destructive interference results in darkness.

For example, the experimentally determined reflectance, $R_\perp$, of GMO–BLM-supported In_2S_3 film as a function of time is shown in Figure 11. Figure 11 also shows the corresponding changes in refractive index (n_s) and optical thickness (d_s) of the film. As seen, n_s rapidly rose to a plateau value, which, in the experiment shown, corresponded to $t = 50$ min and $d_s = 700$ Å. These results can be rationalized by assuming an initial growth of the semiconductor film in the plane of the BLM. The constant value of n_s was obtained only after complete and continuous coverage of the BLM by In_2S_3 film. Subsequent to this point, the film only grew in thickness (d_s), which is reflected in the modulation (Figure 11) of the light intensity of the reflected He–Ne laser beam, as the conditions of constructive or destructive interference are alternately satisfied with time. Growth of the semiconductor film could be controlled by the amount of H_2S injected and by replacing the bathing solution of the BLM (see point E of Figure 11).

The thickness of the BLM-supported, continuous semiconductor film has also been assessed by color comparison, a technique developed some time ago for thin films.[51-54] A comparison of the color of the semiconductor film deposited on the BLM with a color chart constructed for films of different thicknesses of a material with a similar refractive index[54] allowed the assessment of the semiconductor thickness by means of eq 22, where d_o and n_o are the film thickness and refractive index on the color chart corresponding to the observed color.

$$d_s = d_o(n_o/n_s)/\cos \Theta_s \qquad (22)$$

BLM-supported semiconductor thickness was determined more directly with eq 9 and the measured reflectance of the film with a He–Ne laser as described before. We developed our own color chart for In_2S_3 ($n_s = 1.86$ at 6328 A) by observing the interference colors of the film produced by a white light simultaneously with time-dependent thickness measurements. The observed sequential color change of light at normal incidence, yellow gold → orange

(51) Pliskin, W. A.; Conrad, E. E. *J. Phys.* (*Les Ulis, Fr.*) **1964**, *25*, 17.
(52) Pliskin, W. A.; Esch, R. P. *J. Appl. Phys.* **1965**, *36*, 2011.
(53) Blodgett, K. *J. Am. Chem. Soc.* **1935**, *57*, 1007.
(54) Pliskin, W. A. *Solid-State Electron.* **1968**, *11*, 957.

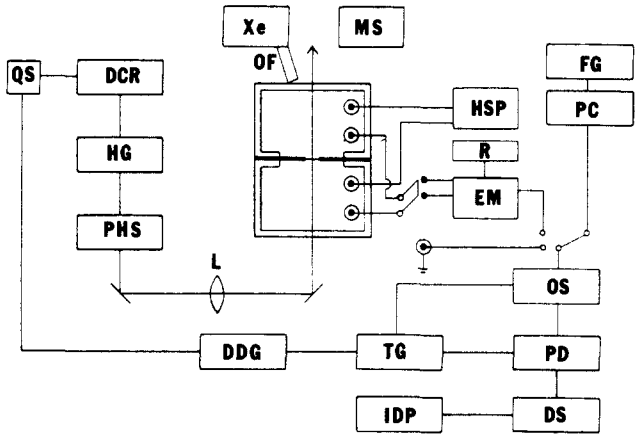

Figure 3. Experimental setup for measuring photoelectric effect from semiconductor-containing BLMs. MS = microscope (Olympus Model PM-10-M); Xe = 150-W xenon lamp; OF = optical fiber guide; HSP = head stage probe (Dagan 8920, 1 GΩ); PC = patch clamp (Model 8900, Dagan Corp.); EM = electrometer (Keithley Model 602); FG = frequency generator (Hewlett-Packard 8116A); QS = Q-switch; DCR = YAG laser (Quanta Ray); HG = harmonic generator (Quanta Ray); PHS = prism-harmonic splitter (Quanta Ray); L = lenses; OS = oscilloscope (Tektronix 2215 and 7633); PD = programmable digitizer (Sony-Tektronix, 390 AD); DDG = digital delay generator (California Avnionic Laboratories, Model 111 AR); T = trigger generator; DS = Zenith (Z-100) computer; IDP = interactive digital plotter (Tektronix 4662).

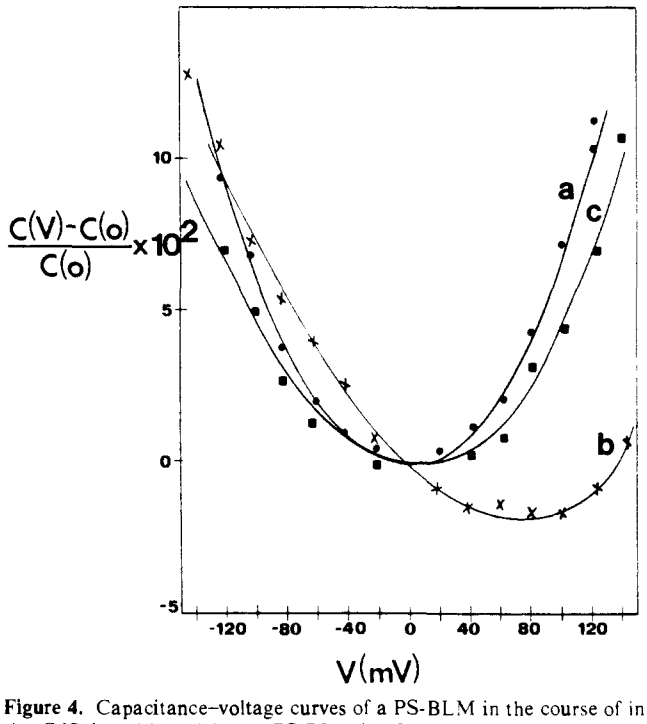

Figure 4. Capacitance–voltage curves of a PS-BLM in the course of in situ CdS deposition: (a) pure PS-BLM in 10 mM KCl bathing solution on both sides of the BLM, (b) 15 min after $CdCl_2$ addition on the cis side ($CdCl_2$ concentration 5.0×10^{-4} M), (c) 5 min after injecting 20 μL of H_2S slowly on the trans side. C_p denotes the measured capacitance of the BLM clamped at potential V.

→ magenta → blue → light blue → bluish yellow → yellow → light pink, upon the in situ generation of In_2S_3 film on the GMO-BLM corresponded to the thicknesses of 0.09, 0.10, 0.13, 0.15, 0.18, 0.21, 0.23, and 0.26 μm, respectively.

The thickness of the BLM-supported, ZnS continuous film[55]

(55) Color change is also influenced by the refractive index of the film. Films with high refractive indices undergo less color change with thickness changes. This was the case for CdS (n = 2.6) and PbS (n_s = 4.3) and the reason for using ZnS (n_s = 1.58) for the illustration of this approach. Lack of availability of color charts for materials having refractive indices similar to these semiconductors has been also responsible for our not performing thickness evaluations for all of the semiconductors generated on BLM surfaces.

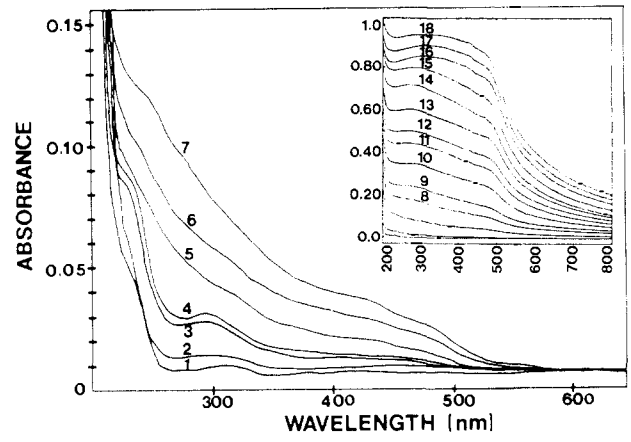

Figure 5. Absorption spectra of CdS particles generated on a GMO-BLM 2 (1), 4 (2), 6 (3), 8 (4), 10 (5), 40 (6), and 90 (7) min after H_2S addition. Spectra 1–4 show structures and absorption edges, which indicate the presence of Q-particles (diameter less than 60 Å with quantum size effects). Photomicrographs taken at this time were completely black. For this experiment, the $CdCl_2$ concentration on the cis side at the beginning was 5×10^{-5} M and 5 μL of H_2S was injected on the trans side. Larger amounts of $CdCl_2$ (2.5×10^{-3} M) and H_2S (25 μL) were used for the experiment shown in the inset. The absorbance curves shown in the inset were measured at 2-min intervals up to curve 14 and then at 4-min intervals. The aqueous solutions in the cell compartments do not show significant absorbance during and after the experiment.

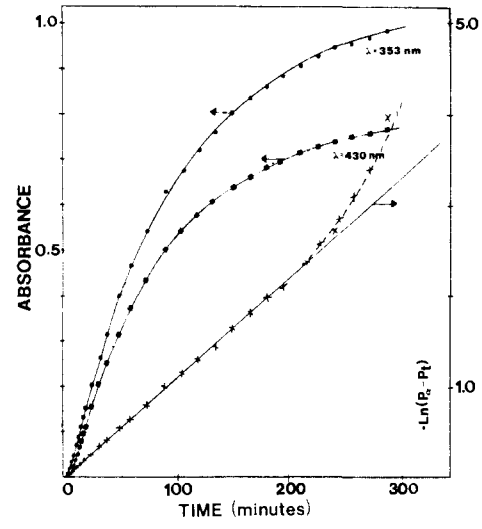

Figure 6. Time evolution of absorbances at 354 and 430 nm in the course of the in situ formation of CdS particles on a GMO-BLM. At time zero, the cis compartment was 2×10^{-3} M in $CdCl_2$ and 25 μL of H_2S was injected in the trans compartment. Plot of $-\ln(P_\infty - P_t)$ against t where P_∞ and P_t are the absorptions at 354 nm after 6 h and after time t is also shown. Linearity of this plot for an initial 3-h period indicates that the formation rate of CdS particles during this time is kinetically first order. The upward trend of the curve from linearity at longer time indicates the presence of an additional slower rate of growth.

with the measured refractive index of 1.58 can be determined by comparing its color with those given by this color chart for an In_2S_3 film with eq 22. Thus, the similar sequential color change observed at the incidence angle of 45° upon the in situ generation of ZnS on the GMO-BLM corresponded to thicknesses of 0.11, 0.15, 0.18, 0.22, 0.25, 0.29, 0.33, and 0.36 μm, respectively.

Capacitance Measurements. Capacitance measurements of a GMO-BLM containing $(5–30) \times 10^{-4}$ M $CdCl_2$ in the cis side at different times subsequent to H_2S addition to the trans side (Figure 12b–d) corresponded to the micrographs shown in Figure 10a–c. Figure 12a illustrates a typical capacitance measurement prior to H_2S addition. GMO-BLMs with 0.8-mm diameters, prior to H_2S addition, had 2-nF capacitance. Subsequent to H_2S addition, but prior to the appearance of the white dots, the BLM capacitance did not change appreciably. Capacitance decreases

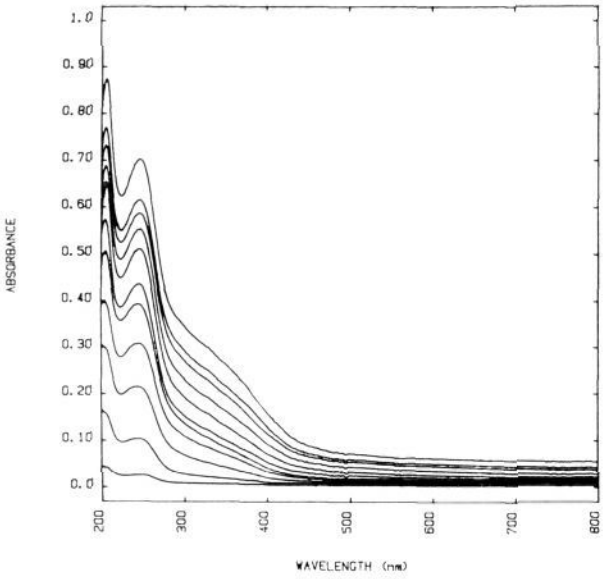

Figure 7. Absorption spectra of InS particles generated on GMO-BLMs. Absorbances were measured at 2-min intervals subsequent to H_2S addition (the initial concentration of $InCl_3$ on the cis side was 2×10^{-3} M, and 25 μL of H_2S was injected on the trans side).

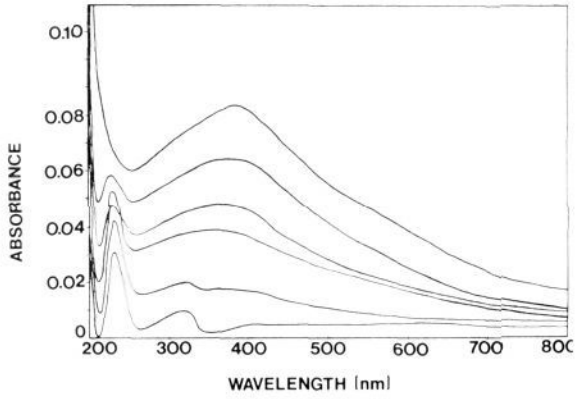

Figure 8. Absorption spectra of PbS particles generated on a GMO-BLM. Absorbances were measured at 5-min intervals subsequent to H_2S addition (the initial concentration of $PbCl_2$ on the cis side was 5×10^{-5} M, and 10 μL of H_2S was injected on the trans side).

were observed to accompany the growth of microcrystalline semiconductors in the BLM matrix. A value of 1 nF for the capacitance was typically observed for well-developed CdS islands in the GMO-BLM matrix.

Presence of a growing semiconductor region in the BLM contributes to the measured capacitance by inducing small charge displacements under the external field. The capacitance of a semiconductor-containing BLM system can be treated as that of an equivalent circuit, consisting of three series contributions: (1) from the semiconductor film, C_s, (2) from the region where the semiconductor film penetrates the BLM, C_h, and (3) from a thinner BLM, $C_{m'}$. The specific capacitance of the semiconductor–BLM system, C_{sm}, is given by eq 23, where d is the

$$C_{sm} = \left(\frac{1}{C_a} + \frac{1}{C_s} + \frac{1}{C_{sm}} \right)^{-1} = \frac{\epsilon_s \epsilon_h \epsilon_m \epsilon_0}{\epsilon_h \epsilon_m d_s + \epsilon_s \epsilon_m h + \epsilon_s \epsilon_h (d - h)} \tag{23}$$

thickness of the BLM prior to semiconductor formation, d_s is the thickness of the semiconductor film, and h is the depth of penetration of the semiconductor film into the bilayer ($h \ll d_s$ vide infra). ϵ_s, ϵ_m, and ϵ_h are the dielectric constants of the semiconductor film, bilayer membrane, and the composite layer of the semiconductor and lipid molecules of the BLM constituting the penetrated volume, respectively.

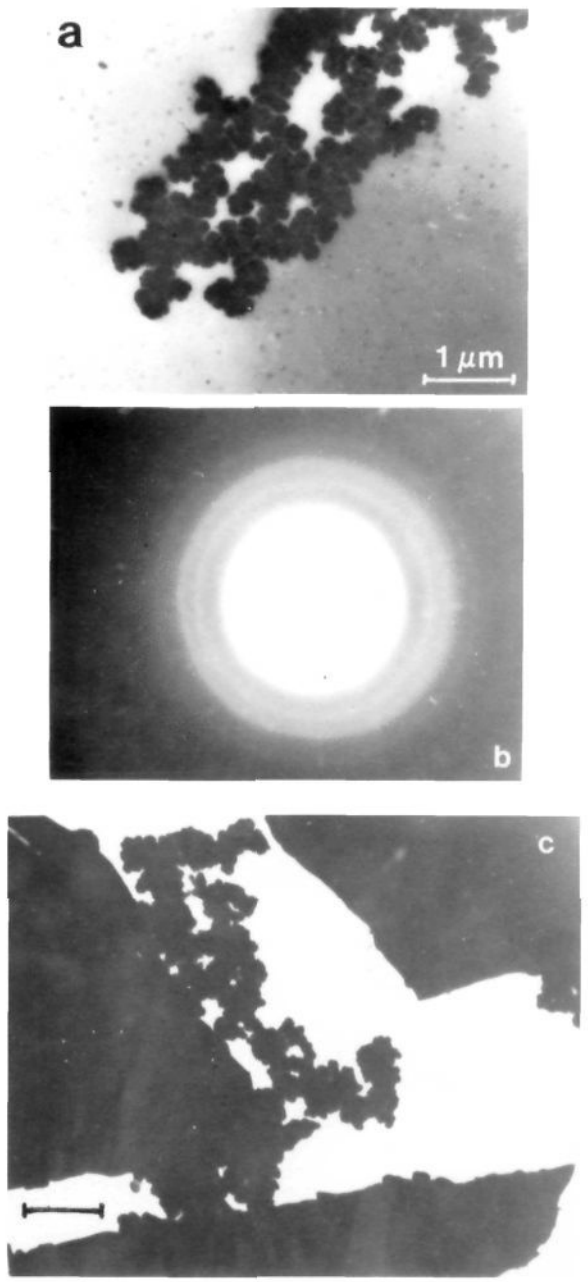

Figure 9. (a) TEM image of the CdS particles produced on a GMO-BLM. The white line is 1 μm long. Diameters of the smaller particles in the background are ca. 100 Å. Clusters of ca. 1000-Å particles are most obvious in the picture. (b) Electron diffraction pattern obtained from these CdS particles. The pattern can be indexed as (111), (220), (311), (400), (422), (440), [(550), (710), (543)] reflections from a cubic, diamond-type lattice with a lattice constant of 5.43 Å. (c) TEM image of the In_2S_3 film at a crack. The black line is 1 μm long.

The relative change in capacitance due to semiconductor formation is given by eq 24. At the beginning of the semiconductor formation, d_s and h are both very small and the denominator in the right-hand side of eq 24 is smaller than the numerator. Thus,

$$\frac{C_{sm} - C_m}{C_m} = \frac{\epsilon_s \epsilon_h d}{\epsilon_h \epsilon_m d_s + \epsilon_s \epsilon_m h + \epsilon_s \epsilon_h (d - h)} - 1 \tag{24}$$

the relative change in capacitance is positive; i.e., the capacitance of the BLM at the beginning increases with semiconductor deposition. However, soon, as the semiconductor thickness increases, the capacitance reaches a maximum value and then starts decreasing as the denominator in eq 24 takes over the numerator. A typical experiment for In_2S_3 film deposition on GMO-BLMs

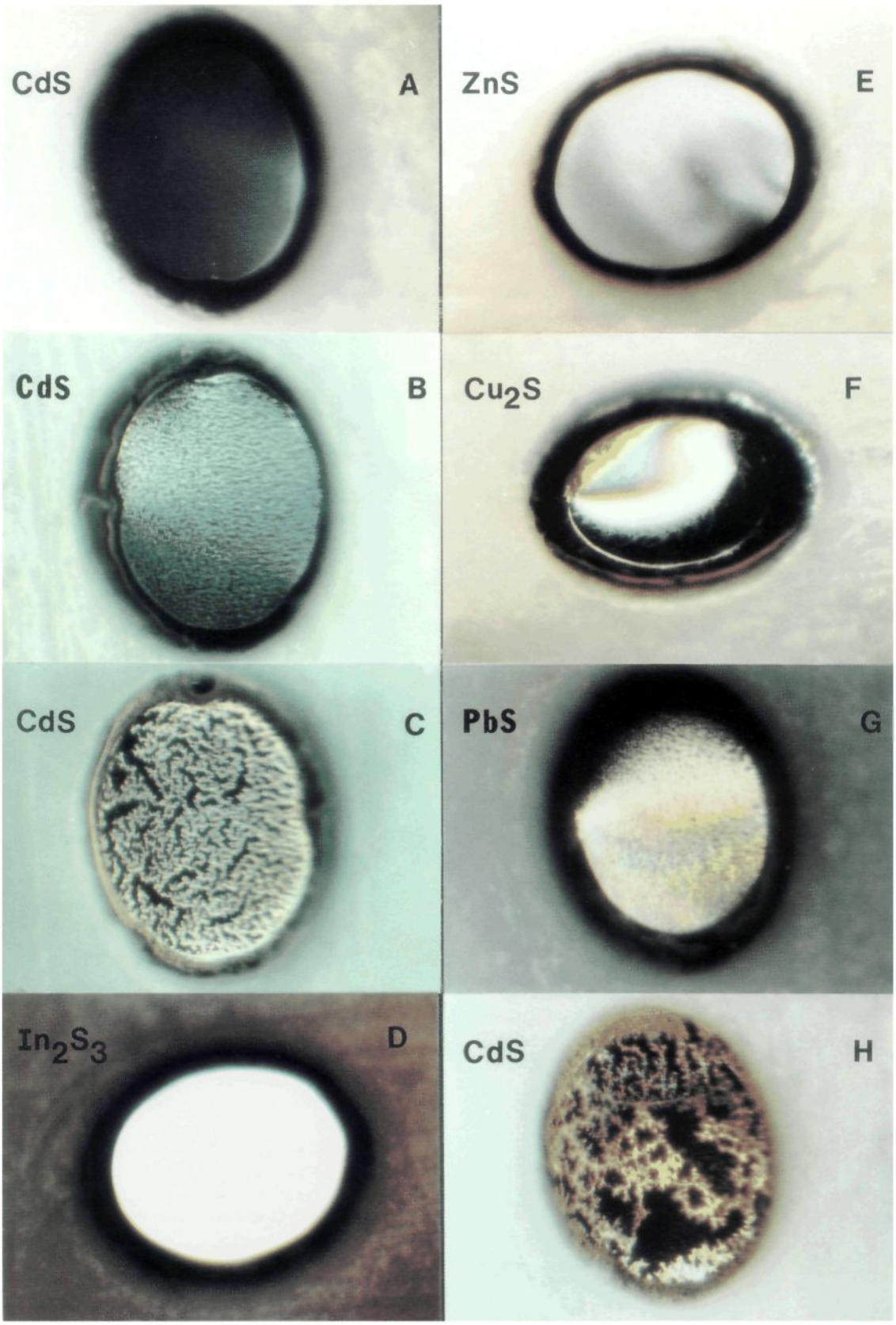

Figure 10. Morphologies of semiconductor particles generated on GMO-BLMs.

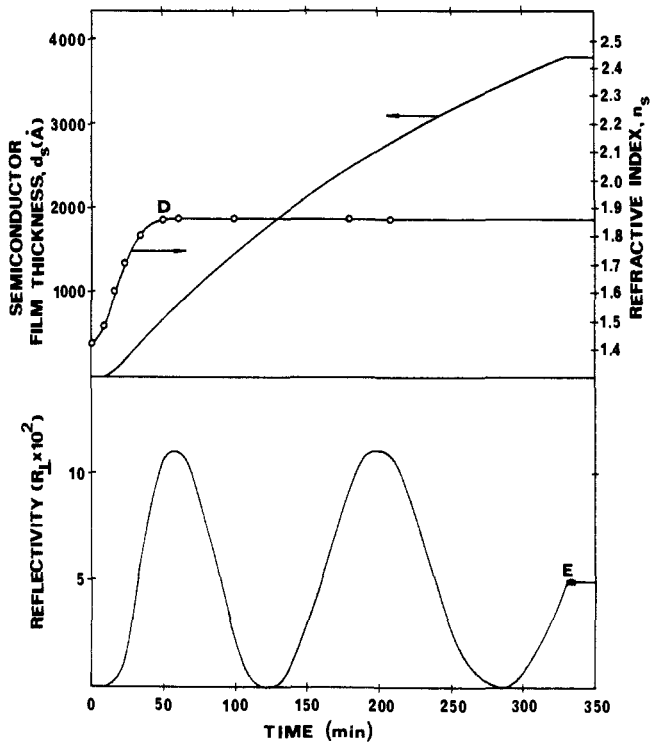

Figure 11. (a) Refractive index calculated from Brewster angle measurements and film thickness for an In_2S_3 film in situ generated on a GMO-BLM at various times after the precursors were added on opposite sides of the BLM. (b) Time variation (plotted by a strip-chart recorder) in intensity of a reflected beam from a He–Ne laser polarized perpendicularly to the incident plane and incident at an angle (Figure 2) of 30°. At point E, the solutions on both sides of the BLM were pumped out and replaced with 0.1 M KCl solution. The film growth, therefore, stopped at E.

is shown in Figure 13. The previously discussed trend in capacitance change is clearly obvious from the data. Measurement of the relative capacitance change and the optical thickness, d_s, simultaneously at various times of semiconductor film formation allows one to compute penetration depth, h, from eq 24. The value of h calculated for In_2S_3 film formation, with $\epsilon_s = 62$, $\epsilon_h = 15.2$,[56] and $\epsilon_m = 2.1$, at various times is also plotted against the semiconductor film thickness. The fact that initially the penetration depth increases steadily with increasing semiconductor thickness indicates an inward force, probably originating in surface tension, exerted by the semiconductor film on the BLM. However, this force is soon counterbalanced by the existing repulsive forces in the BLM, and the penetration depth attains a steady value of 24 Å independent of film thickness. Very similar values of h were found in a number of experiments. The closeness of the steady-state value of h to the thickness of one monolayer and its implications did not escape our attention.

Photoelectric Effects. Photoelectric effects were investigated on asymmetric PS- and GMO-BLM-supported CdS microcrystallites. The cis side contained the semiconductor particles and some Cd^{2+} ions, while H_2S and SH^- were present in the trans side of the BLM. Irradiation with light corresponding to the CdS absorption led to selective energy deposition at only one side of the BLM. The resulting asymmetric charge displacement is expected to manifest in measurable photoelectric effects. Indeed, photoelectric effects have been observed in several BLMs containing asymmetrically distributed pigments.[57] The photovoltage and photocurrent signals observed in CdS-containing PS and GMO-BLMs were found to depend on several factors. These included the amount of CdS present on the BLM, the energy of the incident light, and the composition of the bathing solution. When very small amounts of CdS were present (i.e. corresponding to the absorption spectra 4–5 shown in Figure 5), the observed photovoltages and photocurrents were found to be exceedingly small (10^{-1}–10^{-2} mV and 10–10^2 pA, respectively). With larger amounts of CdS (i.e. corresponding to the absorption spectra 13–15 shown in Figure 5 and photomicrographic picture c in Figure 10), large photovoltages (10–10^2 mV) and photocurrents (10–10^2 nA) were observed. Most experiments were carried out with these latter samples.

In the systems investigated here, the CdS particles were formed in the presence of excess Cd^{2+} ion. These CdS particles are, therefore, expected to have excess Cd^{2+} ions absorbed on the surface (i.e. surface S^{2-} vacancies). This S^{2-} vacancy, V_s^{2+}, acts as a deep electron trap.[58] It exothermally extracts an electron from the full valence band to produce a V_s^+ center and a trapped hole in the valence band. V_s^+ still acts as a deep trap (~0.7 eV) for a conduction band electron.[58-61] The conduction band electrons, e_{CB}^-, generated on excitation of CdS are quickly trapped in V_s^+ vacancies to give V_s^0 centers, which can then transfer an electron to an acceptor present on the surface or can recombine with the nearest preexisting trapped hole or photogenerated hole.

The recombination lifetime of free carriers, e_{CB}^- and h_{VB}^+, formed in CdS microcrystallites subsequent to bandgap excitation has been estimated from luminescence lifetime measurements[57,58] to be ≤10 ps.[62,63] On the other hand, the room-temperature recombination of trapped carriers (e.g. V_s^0 with a valence band hole) gives rise to subbandgap emission whose lifetime ranges between 30 ps and 3 ns, depending upon the depth of the traps.[58,62-64] The lifetime of a trapped carrier can also be considerably enhanced by an interfacial redox reaction that scavenges its partner. Under the condition of low illumination (when only a fraction of the V_s^+ traps are populated), the density of the nonequilibrium carrier at the end of a light pulse of duration t is given by eq 25, where τ is the average lifetime of nonequilibrium

$$\Delta n = \tau \Phi k_s I(1 - e^{-t/\tau}) \quad (25)$$

carriers, Φ is the quantum yield of carrier generation, k_s is the optical absorption coefficient, and I is the light intensity. When $t \gg \tau$, as in the present case, eq 25 simplifies to eq 26, and the

$$\Delta n = \tau \Phi k_s I \quad (26)$$

carrier density at the end of the light pulse is linearly proportional to light intensity, I. However, with increasing light intensity, τ becomes a function of I and the carrier density changes sublinearly with increasing I.[65] Ultimately, when all the traps are filled, the carrier density changes very little with further increase in intensity. The photocurrent signal measured across a CdS-containing GMO-BLM for a 20-ns width, a 353.4-nm laser pulse of energy, and 5 μJ/pulse by clamping the potential across the BLM at 0 V (and thus simulating a short-circuit condition) with the Dagan patch clamp, is shown in Figure 14a. The signal indicates a flow of negative charge in the trans to cis side direction (called forward direction) immediately after the laser pulse. This is followed by a slower charge flow in the reverse direction. The integrated areas under these two halves of the signal (the total charge displaced in any one direction) are almost equal (about 3.2×10^{-12} C), indicating that very little net charge transfer occurred as a result of pulse irradiation. The molecular process that generates the

(56) Landolt-Börnstein *New Series*: Springer-Verlag: Berlin, Heidelberg, New York, Tokyo, 1983; Vol. 111/17f, p 45.
(57) Arrioeta, R.; Arrieta, J. C.; Pachori, P. M.; Popp, A. E.; Huebner, J. S. *Photochem. Photobiol.* **1985**, *42*, 1.
(58) Ramsden, J. J.; Grätzel, M. *J. Chem. Soc., Faraday Trans. 1* **1984**, *80*, 919.
(59) Ramsden, J. J.; Weber, S. A.; Grätzel, M. *J. Phys. Chem.* **1985**, *89*, 2741.
(60) Papavassilion, G. C. *J. Solid State Chem.* **1981**, *40*, 330.
(61) Chestnoy, N.; Harris, T. D.; Hull, R.; Brus, L. E. *J. Phys. Chem.* **1986**, *90*, 3393.
(62) Rossetti, R.; Beck, S. M.; Brus, L. E. *J. Am. Chem. Soc.* **1984**, *106*, 980.
(63) Serpone, N.; Sharma, D. K.; Jamieson, M. A.; Grätzel, M.; Ramsden, J. J. *Chem. Phys. Lett.* **1985**, *115*, 473.
(64) Dounghong, D.; Ramsden, J. J.; Grätzel, M. *J. Am. Chem. Soc.* **1982**, *104*, 2977.
(65) Nosaka, Y.; Fox, M. A. *J. Phys. Chem.* **1986**, *90*, 6521.

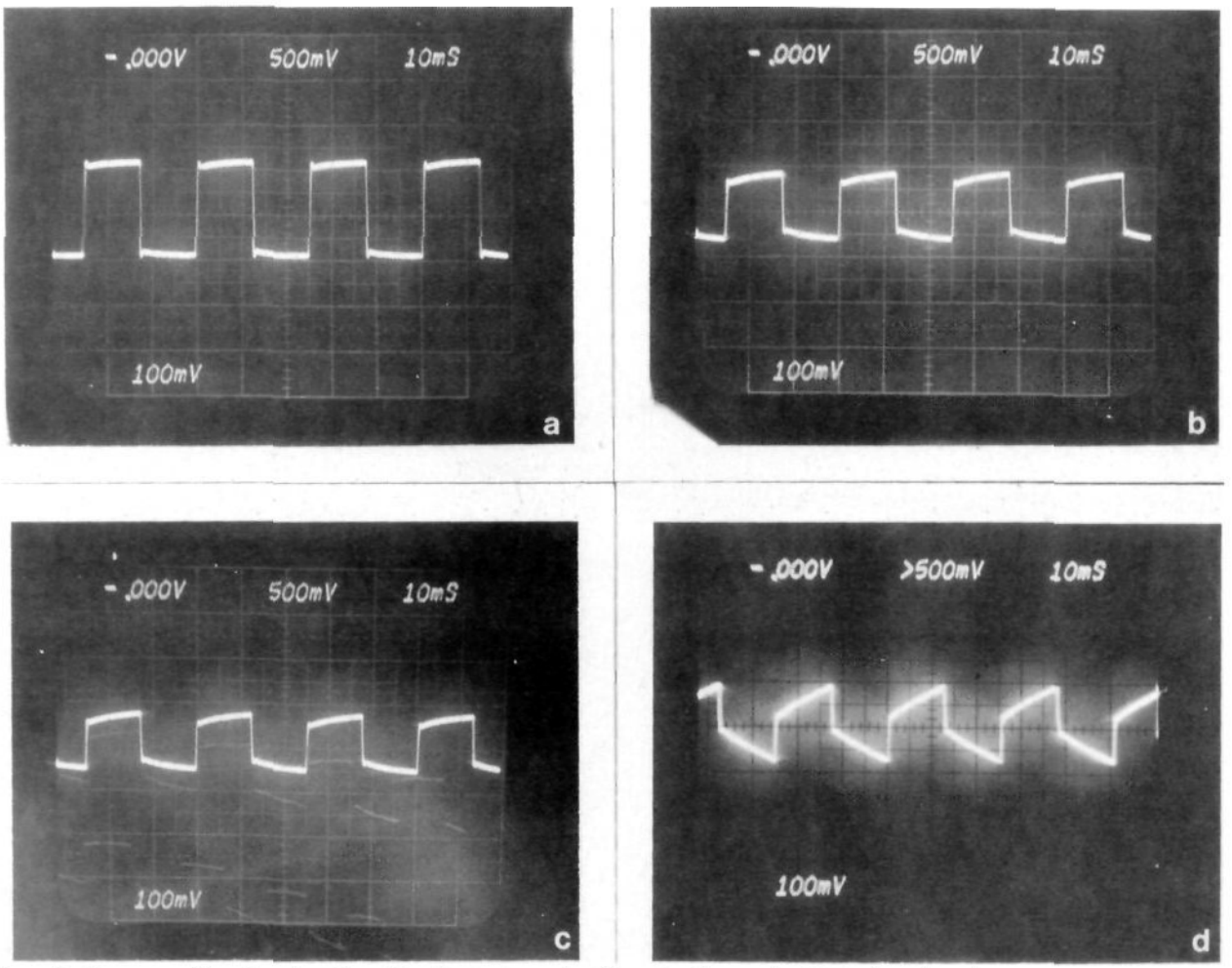

Figure 12. Current waveforms (y scale, 1 div = 500 mV = 1 nA; x scale, 1 div = 10 mS) across the BLM under voltage clamp condition with a triangular clamp potential (amplitude 16 mV, frequency 40 Hz, $dv/dt = \pm 16$ mV/12.5 ms) for simultaneous capacitance and resistance measurements of a GMO-BLM at different stages of CdS growth. In the waveform, the contribution of the capacitance charging current toward the total current is indicated by the sudden change in current when dv/dt changes sign. The change in current with voltage at a constant value for dv/dt indicates the ohmic current flow through the BLM. Part a corresponds to a GMO-BLM. Parts b–d correspond to the CdS formation shown in Figure 10a–c, respectively. Thus, increasing CdS formation on the BLM is associated with a decreasing (except at the very beginning; see text) capacitance and resistance.

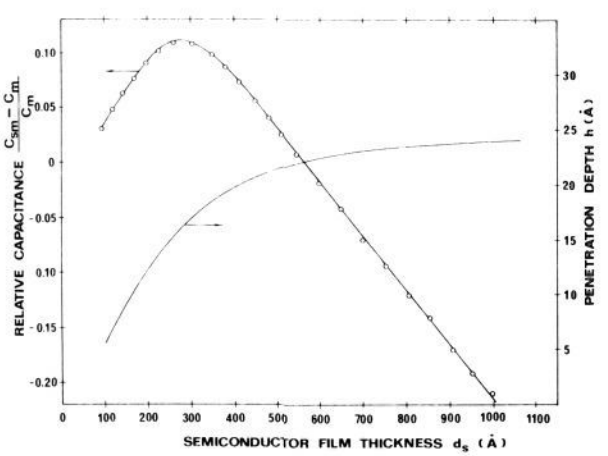

Figure 13. Relative capacitance change as a function of film thickness in the course of the growth of an In_2S_3 film on a GMO-BLM in a typical experiment. The magnitude of penetration depth, h, calculated from eq 24 is also plotted as a function of film thickness.

photocurrent in the forward direction is the reduction of dissolved oxygen in the solution by the V_s^0 centers formed in the CdS microcrystallites as a result of irradiation. Transient formation of O_2^- ion has been observed by spin trapping and ESR experiments on bandgap-irradiated, aqueous CdS dispersions.[66,67] Addition of 1×10^{-4} M methylviologen chloride, $MVCl_2$, a stronger electron acceptor than O_2, to the cis side solution increased the magnitude of the photocurrent in the forward direction by about 3–4-fold. Recombination of O_2^- or $MV^{\cdot+}$ (in presence of $MVCl_2$) with the photogenerated hole in CdS gives rise to the current in the backward direction observed in the latter part of the signal. Thus, photoinduced charge separation and recombination in the cis, aqueous BLM interface gave rise to the observed ac photoelectric effect, which has also been named chemical capacitance effect.[68-70] There is little net chemical change of the system as a result of irradiation. The maximum quantum yield of transient charge separation obtained can be calculated to be 2×10^{-6} on the basis of the number of incident photons. An attempt to expand the time scale and lower the instrument response time by setting the patch clamp at wide-band filter and high-frequency boost resulted in the signal shown in Figure 14d. No attempt has been made to extract electron-transfer rates from these

(66) Harbour, J. R.; Han, M. L. *J. Phys. Chem.* **1977**, *81*, 1791.
(67) Harbour, J. R.; Wolkow, R.; Han, M. L. *J. Phys. Chem.* **1981**, *85*, 4026.
(68) Mauzerall, D. In *Light-Induced Charge Separation in Biology and Chemistry*; Gerischer, H., Katz, J. J., Eds.; Dahlem Konferenzen: Berlin, 1979; pp 241–257.
(69) Hong, F. T.; Mauzerall, D. *Proc. Natl. Acad. Sci. U.S.A.* **1974**, *71*, 1564.
(70) Hong, F. T. *Photochem. Photobiol.* **1976**, *24*, 155.

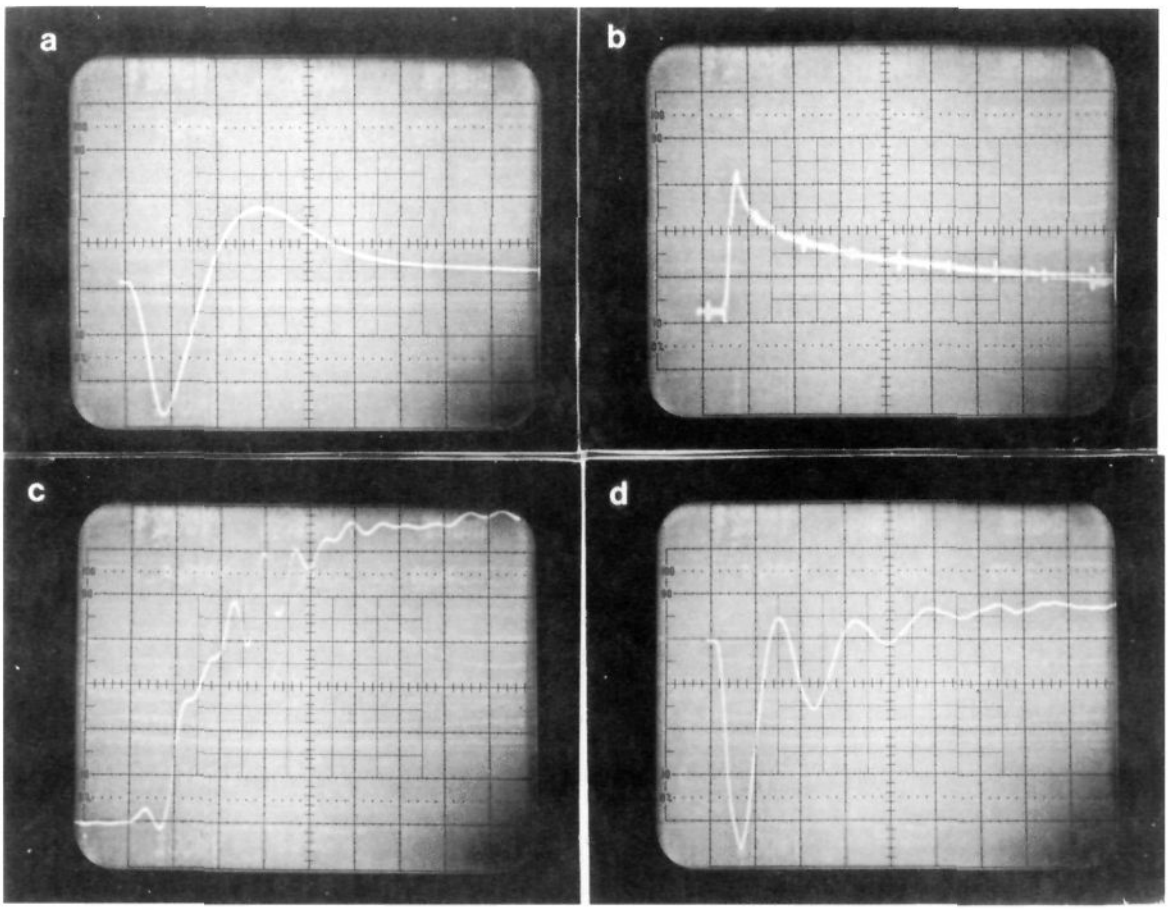

Figure 14. Photoelectric effects measured from CdS-containing GMO-BLMs under different conditions. Irradiation in all cases was done with 20-ns pulses of 353.4-nm light (third harmonic) from a Nd-YAG laser from the trans side of the BLM. Several different CdS-containing BLMs were used. *(a) Photocurrent recorded with a Dagan patch clamp maintaining a zero potential difference across the BLM* (current scale, 5 nA/div; time scale, 200 μs/div). A negative current in our experimental setup indicates an electron flow in trans → cis direction. The laser energy was 5 μJ/pulse. (b) Photovoltage signal recorded with the Keithley electrometer under open-circuit condition (voltage scale, 50 mV/div; time scale, 20 μs/div). The electrode on the cis side (CdS-containing side) became negative. The laser energy was 1 μJ/pulse. (c) The rising edge of the photovoltage signal measured by directly connecting the electrodes to the input of an oscilloscope of 1-MΩ input resistance (voltage scale, 20 mV/div; time scale, 0.2 μs). The laser energy was 1 μJ/pulse. (d) Rising edge of the photocurrent signal measured with patch clamp in the high-frequency boost and wide-band filter mode maintaining a zero potential difference across the BLM (current scale, 10 nA/div; time scale, 5 μs/div).

signals as they are obviously distorted by the apparatus time constants. The dependence of the magnitude of the observed photocurrent in a forward direction on the laser pulse intensity for a certain constant amount of CdS on GMO BLMs is shown in Figure 15. The observed dependence reflects well the variation of the carrier density at the end of the pulse with laser intensity as discussed earlier.

The photovoltages developed in these experiments were simultaneously measured under open-circuit condition with an electrometer (10^{14}-Ω input impedance) or with an oscilloscope (input resistance 10^6 Ω and capacitance 20 pF), and displayed in parts b and c in Figure 14. The actual rise time of the photovoltage signal, which is related to the electron-transfer rate, once again could not be determined because of the comparatively large instrument-response time. However, the direction of the observed photovoltage (the cis side of the BLM becoming negative) and its dependence on the light intensity (Figure 15) support the postulated mechanism.

Although most of the charge transfer that initially takes place is cancelled by reverse transfer, a small amount of net charge transfer takes place through the BLM. This net transfer gives rise to a small photovoltage response of the system under steady-state irradiation condition as shown in Figure 16a. The observed photovoltage here is considerably smaller than that observed in Figure 15. The fact that the electrode on the cis side becomes negative shows that the net electron transfer also takes place in the forward direction. Presumably, the SH^- ions act as donors on the trans side to maintain a steady voltage. The amount of the chemical reaction is, however, very small, as both the membrane resistance and outside circuit resistance are very high.

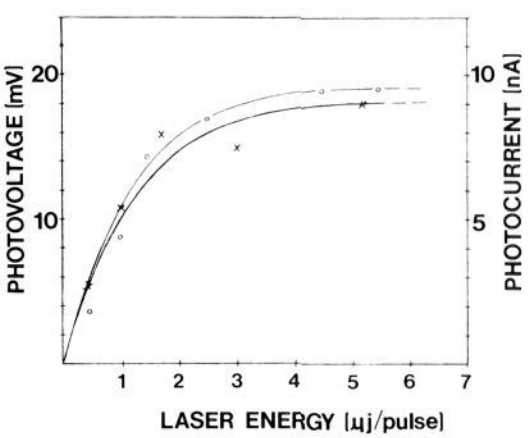

Figure 15. Dependence of the magnitude of the observed photoelectric effect on the energy of the laser pulse incident on the CdS-containing GMO-BLM. The photovoltage was measured with an electrometer and the photocurrent with a patch clamp. The laser was focused on a 0.3-mm^2 area on the BLM. The experiment was carried out with a BLM containing a much smaller amount of CdS than those described in Figure 15b, where much larger photoelectric signals were observed.

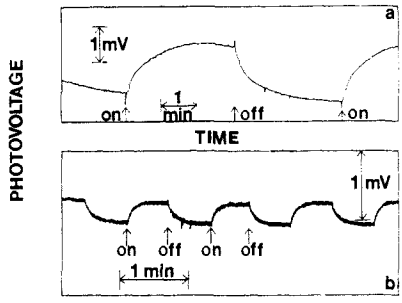

Figure 16. Photovoltage developed on irradiating a In_2S_3-containing GMO-BLM by a continuous-light source: (a) after forming In_2S_3 in situ by adding $InCl_3$ in the cis and H_2S in the trans side of the GMO-BLM; (b) subsequent to the addition of 10 μL of 0.1 M $K_4Fe(CN)_6$ in the cis side. Light from a 150-W xenon lamp was guided by an optical fiber and focused on the BLM. In both cases, the electrode on the cis side acquires a negative electrical potential upon illumination.

Addition of ferrocyanide ion, $Fe(CN)_6^{4-}$, which acts as a strong hole acceptor on the cis side, was found to considerably decrease the photovoltage (Figure 16b), further confirming the above mechanism of charge transfer. This is also substantiated by the fact that in the presence of ferrocyanide the attainment of steady state is much faster, as the photogenerated holes are scavenged by ferrocyanide ions present in solution in a much higher concentration than O_2^- ions in the same side.

Photopolymerization. CdS-sensitized polymerization of STYRS-BLMs has been observed by incorporating preformed CdS colloidal particles stabilized with sodium hexametaphosphate[30] into a BLM made from STYRS surfactant. Attempts to produce CdS in situ in BLMs made from STYRS by using a neutral solution of $Cd(EDTA)^{2-}$ on cis side of the BLM and H_2S on the trans side has, in most cases, been unsuccessful due to membrane collapse. Therefore, the photopolymerization experiments were carried out by forming the BLM in a bathing solution containing small CdS particles of diameter ~50 Å.[30] The 260-nm absorption band of the STYRS surfactant arises predominantly from the electron excitation in the styryl group and, therefore, absorption at this wavelength gives a measure of monomer concentrations in the BLM.

Irradiation in these photopolymerization experiments was done at wavelengths greater than 350 nm where STYRS molecules do not absorb. The absorption of the light in the 350–480-nm wavelength range resulted in bandgap excitation of these CdS particles. Decreasing absorption at 260 nm indicates the progress of sensitized polymerization (Figure 17) with irradiation. The mechanism of polymerization of similar CdS-sensitized polymerization of vesicles made from STYRS surfactant has been recently established in our laboratories.[31] The electrons are scavenged by oxygen molecules present in the solution whereas the holes initiate the polymerization via the formation of styryl cation.[31] The mechanism in BLMs should be very similar.

It has recently been shown that, with DHP vesicle incorporated CdS particles containing methylviologen, bandgap irradiation results in the reduction of only those MV^{2+} molecules that are absorbed on the surface of the particle in the presence of an efficient hole acceptor, such as benzyl alcohol.[23] This is because of the very short (3 ns or less) lifetime of the photogenerated carriers in CdS. We suggest, therefore, that those CdS particles that are present on the BLM are the only effective photosensitizers. The present case, therefore, strongly indicates the occurrence of a chemical reaction between the surfactant molecules and the semiconductors present on the BLM surface.

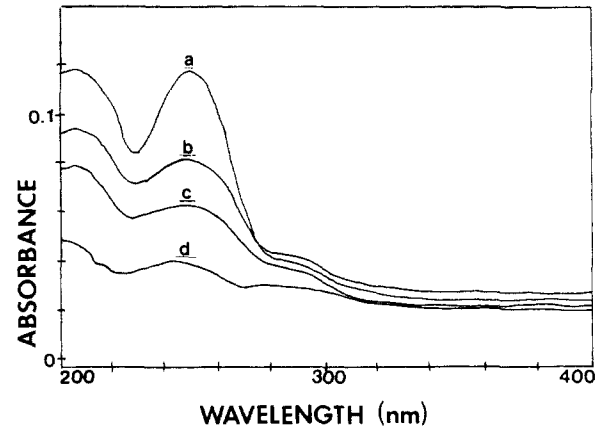

Figure 17. Bandgap excitation of CdS particles incorporated into BLMs prepared from STYRS by light of wavelength longer than 350 nm for 0 (a), 2 (b), 4 (c), and 8 (d) min resulted in the polymerization of the styrene moiety of the STYRS surfactant molecules.

Conclusion

Formation and characterization of crystalline semiconductor particles on BLMs have been reported in the present work. Advantages of this approach are manifold. The physical arrangement permits controlled particle growth in an environment (under ultrapure, dust-free water) where impurities can be conveniently controlled and allows simultaneous observations by electrical, spectroscopic, and microscopic techniques. These, in turn, can lead to the elucidation of the mechanisms involved in nucleation and crystalline semiconductor and film formations. Information can also be obtained on the dimensionalities and morphologies that govern semiconductor formation and stabilities.

The BLM serves as an ultrathin (45 ± 10 Å), supporting membrane matrix. Evidence has been presented here for maximum semiconductor penetration of 24 Å into the membrane. Thus, the transmembrane distance is decreased to a range (21 ± 10 Å) where electron transfer becomes feasible.[71,72] Indeed, photoelectron transfers across GMO-BLM-supported In_2S_3 have been documented here.

Semiconductor incorporation has markedly increased the stability of the BLMs: they lasted for several days. Even the bathing solution could be removed without disturbing the BLM-supported semiconductor. Furthermore, the preparation of arrays of 30–35 BLM-supported semiconductors on a copper grid launched these investigations into the realm of solid-state chemistry. This approach can potentially lead to viable methods for the preparation of microsized semiconductors, thin semiconductor junctions, and other electronic components. Exploitation of these ideas is the subject of our current intensive scrutiny.

Acknowledgment. Support of this work by the National Science Foundation and by the Department of Energy is gratefully acknowledged.

Registry No. GMD, 25496-72-4; STYRS, 88703-85-9; $(STYRS)_x$, 98065-26-0; $CdCl_2^-$, 10108-64-2; $Hg(NO_3)_2$, 10045-94-0; Cu_2Cl_2, 7758-89-6; $ZnCl_2$, 7646-85-7; $Pb(NO_3)_2$, 10099-74-8; $CuSO_4$, 11115-78-9; $CuCl_2$, 7447-39-4; H_2S, 7783-06-4; $InCl_3$, 10025-82-8; CdS, 1306-23-6; Cu_2S, 22205-45-4; PbS, 1314-87-0; ZnS, 1314-98-3; HgS, 37251-50-6; In_2S_3, 12030-24-9; CuS, 1317-40-4.

(71) Tsuchida, E.; Kaneko, M.; Nishide, H.; Hoshino, M. *J. Phys. Chem.* **1986**, *90*, 2283.
(72) Lee, L. Y. C.; Hurst, J. K. *J. Am. Chem. Soc.* **1984**, *106*, 7411.